Design of Switchable Chimeric Antigen Receptor T Cells Targeting Breast Cancer

Yu Cao, David T. Rodgers, Juanjuan Du, Insha Ahmad, Eric N. Hampton, Jennifer S. Y. Ma, Magdalena Mazagova, Sei-hyun Choi, Hwa Young Yun, Han Xiao, Pengyu Yang, Xiaozhou Luo, Reyna K. V. Lim, Holly M. Pugh, Feng Wang, Stephanie A. Kazane, Timothy M. Wright, Chan Hyuk Kim,* Peter G. Schultz,* and Travis S. Young*

Abstract: *Chimeric antigen receptor T (CAR-T) cells have demonstrated promising results against hematological malignancies, but have encountered significant challenges in translation to solid tumors. To overcome these hurdles, we have developed a switchable CAR-T cell platform in which the activity of the engineered cell is controlled by dosage of an antibody-based switch. Herein, we apply this approach to Her2-expressing breast cancers by engineering switch molecules through site-specific incorporation of FITC or grafting of a peptide neo-epitope (PNE) into the anti-Her2 antibody trastuzumab (clone 4D5). We demonstrate that both switch formats can be readily optimized to redirect CAR-T cells (specific for the corresponding FITC or PNE) to Her2-expressing tumor cells, and afford dose-titratable activation of CAR-T cells ex vivo and complete clearance of the tumor in rodent xenograft models. This strategy may facilitate the application of immunotherapy to solid tumors by affording comparable efficacy with improved safety owing to switch-based control of the CAR-T response.*

Adoptive immunotherapy using chimeric antigen receptor T (CAR-T) cells is a promising approach for cancer treatment.[1–3] Clinical trials have demonstrated marked antitumor responses for patients with hematological malignancies, including those who have failed conventional therapies.[4–7] Despite these promising early results, significant challenges still exist. For example, leukemia and lymphoma patients treated with CD19-specific CAR-T cells have suffered severe cytokine release syndrome (CRS) owing to the rapid activation and expansion of CAR-T cells upon encountering CD19-positive cells, and developed long-term B-cell aplasia owing to the persistence of the CAR-T response.[4,8,9] The treatment of solid tumors has proven even more problematic due to on-target, off-tumor activity of CAR-T cells that has resulted in damage to healthy tissue.[10] In other solid tumor trials, CAR-T cells have demonstrated insufficient efficacy.[11,12] Thus, it has become increasingly appreciated that the treatment of solid tumors with CAR-T cell therapy requires robust methods for systematically optimizing and precisely controlling the engineered cells to provide an effective therapy with mitigated risks to the patient. One method that has been proposed is a safety switch that can eliminate engineered cells in the case of an adverse event.[13] However, this strategy results in irreversible loss of therapeutic cells from circulation and does not solve the intrinsic lack of control associated with conventional CAR-T cell therapy.

To control CAR-T cell activation, we and others have previously developed antibody-based switch molecules that control the activation, antigen specificity, and phenotype of CAR-T cells by the formation of a switch-dependent immunological synapse.[14–16] This switchable CAR-T (sCAR-T) cell platform relies on a sCAR that is specific for a bio-orthogonal antigen (not present in normal tissue), and a recombinant antibody-based switch that confers tumor specificity and also contains the sCAR antigen. The activity of these sCAR-T cells is entirely dependent on the presence of the switch molecule. Recently, we reported the development of two sCAR platforms that utilized either semi-synthetic switches, generated by site-specific chemical conjugation of the targeting antibody with the small molecule fluorescein isothiocyanate (FITC), or fully recombinant switches constructed from genetic fusion of the targeting antibody with a short peptide neo-epitope (PNE) derived from the GCN4 peptide sequence.[15,16] sCAR-T cells redirected by either FITC- or PNE-tagged switches efficiently cleared CD19+ Nalm-6 tumors in murine xenograft models with reduced toxicity by virtue of the ability to titrate the sCAR-T cell response. Additionally, sCAR-T activity could be terminated by removal of the switch. Moreover, this platform can allow

[*] Dr. Y. Cao, I. Ahmad, Dr. S. H. Choi, Dr. H. Y. Yun, Dr. H. Xiao, X. Luo, Prof. P. G. Schultz
Department of Chemistry and
The Skaggs Institute for Chemical Biology
The Scripps Research Institute
10550 N Torrey Pines Rd, La Jolla, CA 92037 (USA)
E-mail: Schultz@scripps.edu

Dr. D. T. Rodgers, Dr. J. Du, E. N. Hampton, Dr. J. S. Y. Ma, Dr. M. Mazagova, Dr. P. Yang, Dr. R. K. V. Lim, H. M. Pugh, Dr. F. Wang, Dr. S. A. Kazane, Dr. T. M. Wright, Dr. C. H. Kim, Prof. P. G. Schultz, Dr. T. S. Young
California Institute for Biomedical Research
11119 N Torrey Pines Rd, La Jolla, CA 92037 (USA)
E-mail: chkim@calibr.org
          tyoung@calibr.org

Dr. S. H. Choi
Present address: Daegu-Gyeongbook Medical Innovation Center
80 Chembok-ro, Dong-gu, Daegu, 41061 (Korea)

Dr. C. H. Kim
Present address: Department of Biological Sciences
Korea Advanced Institute of Science and Technology
291 Daehak-ro, Yuseong-gu, Daejeon, 34141 (Korea)

Supporting information for this article can be found under:
http://dx.doi.org/10.1002/anie.201601902.

one universal CAR-T cell to be redirected to target heterogeneous or resistant tumors with multiple distinct switches, which should further improve the effectiveness of this therapeutic modality.[15–19]

Herein, we extend this methodology to target Her2-expressing breast cancer cells. To generate anti-Her2 switches, the FITC or PNE peptide was introduced into the anti-Her2 antibody fragment Fab (clone 4D5) at defined sites in the variable or constant regions. These positions were chosen to vary the distance and orientation between the CAR and tumor antigen to optimize the immunological synapse. For the FITC-based switches, a bio-orthogonal genetically encoded unnatural amino acid was used to site-specifically conjugate FITC to 4D5 Fab. Briefly, a mutant 4D5 Fab with a TAG nonsense codon at the desired sites was co-expressed in *Escherichia coli* (*E. coli*) with an orthogonal *Methanococcus jannaschii*-derived tRNA/aminoacyl-tRNA synthetase pair that selectively incorporates *p*-azidophenylalanine (pAzF) into proteins in response to the TAG codon. Based on previous experiments, pAzF was individually incorporated at light chain residues (LG68X or LS202X) or heavy chain residues (HS75X or HK136X) to generate four monovalent switches (Figure 1 A).[15] In addition, two bivalent switches were constructed with pAzF at both LG68X and HS75X, or

LS202X and HK136X. To conjugate FITC to the Fab, a linker-modified FITC molecule containing a cyclooctyne group (BCN-PEG4-FITC) was attached through "Click" reaction[20,21] (Supporting Information, Figure S1). Conjugation reactions proceeded to > 95 % completion as determined by SDS-PAGE gel (Figure S2 A) and mass spectrometry (MS; Figure S3 and Table S1).

To generate PNE switch molecules, we grafted the PNE peptide sequence to the N- or C-terminus of the 4D5 Fab heavy chain or light chains to create the light chain N-terminal (LCNT), light chain C-terminal (LCCT), heavy chain N-terminal (HCNT), or heavy chain C-terminal (HCCT) switches (Figure 1 A). A GGGGS peptide linker was used to separate the peptide tag from the Fab. To create bivalent switches, the PNE was grafted onto either the N- or C-terminus of the heavy and light chains to create NTBV or CTBV, respectively (Figure 1 A). Proteins were expressed in HEK293 suspension cells and further purified to > 95 % homogeneity as confirmed by SDS-PAGE gel (Figure S2 B). MS analysis confirmed that the PNE fusions were not subject to post-translational modification or proteolysis (Figure S4 and Table S2). The binding affinity of all of the switches to SKBR3 (Her2 3+, clinical immunohistochemistry score), MDA-MB453 (Her2 2+), MDA-MB231, MDA-MB435 (Her2 1+), and MDA-MB468 (Her2 0)[22] cancer cells was assessed by flow cytometry. As shown in Figure S5, FITC- and PNE-based switches bound to Her2-expressing cancer cells to a similar extent as wild-type 4D5 Fab (Table S3 and S4). Importantly, these switch molecules did not bind to MDA-MB468 (Her2-negative) cancer cells, confirming the specificity of the modified 4D5 Fab-based switches.

We have previously engineered sCARs using high affinity scFvs for FITC or the PNE[23,24] in 4-1BB-based second generation CAR backbones[25] (Figure 1 B). For the PNE sCAR, we further showed that a short 12 amino acid hinge region (which connects the scFv to the transmembrane domain), derived from a dimeric mutant (S228P) of the IgG4 hinge (IgG4m), afforded greater activity than a longer 45 amino acid CD8 hinge region that is used in many conventional CAR constructs.[16] Therefore, for both the FITC and PNE sCARs, we generated constructs harboring both the IgG4m and CD8 hinges (Figure 1 B). Comparable sCAR expression (transduction efficiency of ~ 60 %) for all four of the constructs on the surface of T cells was confirmed by flow cytometry, consistent with previous results.[15,16] We then tested the ability of the sCAR-T cells with CD8 or IgG4m hinges to bind to their corresponding anti-Her2 switches. As shown in Figures S6 and S7, all of the switches bound to their corresponding sCAR-T cells with similar affinities. The wild-type 4D5 Fab or an unrelated switch antibody, did not bind to either sCAR-T cell, demonstrating the specificity of the sCARs for their respective tags (Figure S8).

To determine the optimal switch/sCAR combination for targeting Her2-expressing cells, we measured sCAR-T cell activation with monovalent (HS75X and LS202X for FITC; HCNT and LCCT for PNE) and bivalent (LG68X/HS75X and LS202X/HK136X for FITC; NTBV and CTBV for PNE) switches against breast cancer cells with varying levels of
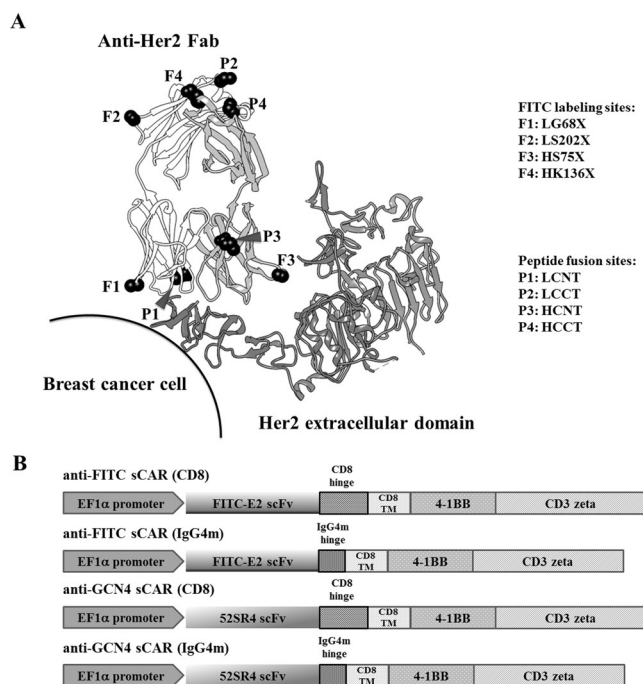

Figure 1. Construction of FITC or PNE (GCN4) anti-Her2 Fab switches. A) Crystal structure of the anti-Her2 4D5 Fab bound to Her2 (dark gray) showing the heavy (light gray) and light (white) chains. Positions of the four amino acids that were individually mutated in separate constructs to encode pAzF- for FITC-conjugation are labeled with "F". The location of the two N-terminal and two C-terminal positions that were grafted with the PNE (GCN4) are labeled with "P". The structure is derived from crystal structure Protein Data Bank ID 1N8Z. B) Representation of anti-FITC and anti-PNE (GCN4) sCARs containing the CD8 signaling sequence, corresponding scFv, extracellular hinge region (CD8 or IgG4m), CD8 transmembrane domain, 4-1BB co-stimulatory domain, and CD3ζ signaling domain.

Her2 expression (Figures S9 and S10).[22] In general, switches with FITC or PNE placed distal to the antigen-binding domain provided the greatest activation. This result is consistent with the membrane proximal epitope of the Her2-specific 4D5 Fab which likely requires extended distance between the sCAR-T cell and target cell to achieve an optimal synapse geometry (compared with switches against CD19 previously developed from the FMC63 Fab). For anti-FITC sCAR-T cells, the bivalent LS202X/HK136X switch induced the highest sCAR-T activation, and this trend was most apparent on Her2 1+ cancer cells. As shown in Figure S9, the CD8 hinge-based anti-FITC CAR-T cells afforded greater sCAR-T cell activation than the IgG4m hinge-based sCAR-T cells for all of the FITC switch designs, as determined by CD69/CD25 upregulation and inflammatory cytokine release (IL-2, IFN-γ, and TNF-α). Interestingly, for anti-PNE sCAR-T cells the same hinge was not optimal for all representative PNE-based switches tested (Figure S10). The anti-PNE sCAR harboring the CD8 hinge showed the greatest T cell activation and cytokine release when used with N-terminal (HCNT) PNE switches, but when the PNE was grafted onto the C-terminus (LCCT), the IgG4m hinge-based anti-PNE sCAR showed the best response. In agreement with the T-cell activation results, anti-FITC sCAR-T cells with the CD8 hinge were more cytotoxic than those with the IgG4m hinge (Figure 2 A), while anti-PNE sCAR-T cells with the IgG4m hinge were more cytotoxic than those with the CD8 hinge (Figure 2 B). Notably, differences in cytotoxicity for CD8 versus IgG4m hinges were most apparent for Her2 1+ compared with Her2

3+ and Her2 2+ cells (Figure S11). The small number of immunological synapses formed by the low antigen density cells likely magnifies the requirement for optimal complex formation to produce efficient target cell cytotoxicity. Cytotoxicity by dose titration of all of the switch designs against Her2 1+ cells confirmed that the FITC LS202X/HK136X with anti-FITC CAR-T cells harboring CD8 hinge (EC_{50} ranging from 2.9 ± 0.2 to 18.3 ± 2.4 pM; Figure S12 and Table S5) and PNE CTBV with IgG4m-based anti-PNE CAR-T cells (EC_{50} ranging from 2.0 ± 0.2 to 4.0 ± 0.7 pM; Figure S13 and Table S6) provided the greatest level of cytotoxicity.

To understand the basis for hinge preference in FITC- and PNE-based switches, we examined the structural differences between FITC- and PNE-based switches. As shown in Figure S14 A, the LS202X and HK136X sites of FITC attachment are predicted to be approximately 24.4 Å apart, while the LCCT and HCCT grafting positions for the PNE are only 11.6 Å apart (Figure S14 B). Because the linkers used for FITC small molecule conjugation (PEG4) and PNE grafting (GGGGS) are comparable in length, the differential activity may be due to the differences in the location of FITC conjugation sites relative to the PNE grafting location. To test this possibility, we constructed a bivalent FITC switch by conjugation to residues LG212X and HK221X, which are approximately 11.6 Å apart in the constant domain, and distal to the antigen binding region (Figure S14 C). As shown in Figure S15, the LG212X/HK221X FITC switch was more cytotoxic with the IgG4m hinge compared to the CD8 hinge in the FITC sCAR-T cell against Her2 1+ cells. Similarly, this
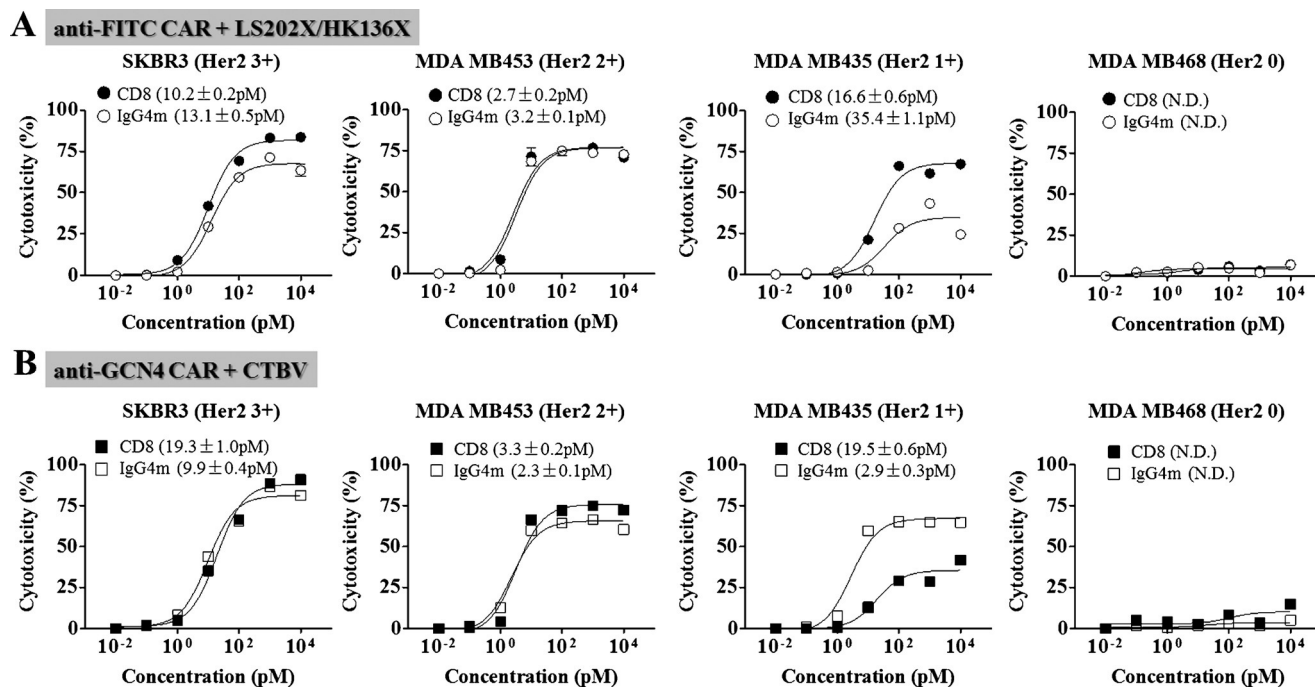
Figure 2. In vitro cytotoxicity of sCAR-T cells harboring the CD8 or IgG4m hinges with bivalent switches. A) FITC- or B) GCN4-specific sCAR-T cells containing different hinges were incubated with SKBR3 (Her2 3+), MDA-MB453 (Her2 2+), MDA-MB435 (Her2 1+), or MDA-MB468 (Her2 0) cancer cells at an E:T = 10:1 ratio with serial dilution of FITC switch LS202X/HK136X or GCN4 switch CTBV. Cytotoxicity was assayed after 24 h by measuring the amount of lactate dehydrogenase (LDH) released into cultured media. The EC_{50} values (mean ± SD) were determined and listed in parenthesis in the legend inserts. N.D. indicates not determined.

new FITC switch exhibited more robust sCAR-T cell activation and greater release of inflammatory cytokines with anti-FITC sCAR-T cell harboring the IgG4m hinge (Figure S16). This result is similar to that of the PNE-based CTBV switch with roughly the same geometry. Collectively, these results indicate that concurrent design of the sCAR hinge and switch labeling sites is required to achieve the optimal distance and orientation for sCAR-T cell activation.

We next compared the in vitro cytotoxicity of the optimal switch/sCAR pair with that of conventional anti-Her2 CAR. The 4D5 scFv and CD8 hinge were used for the conventional anti-Her2 CAR, as previously reported.[26] For this experiment, 50 pM of the FITC LS202X/HK136X or PNE CTBV switch was used with the CD8 hinge FITC CAR or the IgG4m hinge CAR, respectively. As shown in Figure S17, sCAR-T cells killed Her2 cancer cells with comparable efficacy to the conventional CAR-Her2 across all E:T ratios tested. Both sCAR-T cells and conventional CAR-T cells showed good selectivity for Her2 cells with only minor cytotoxicity towards Her2 0 MDA-MB468 cells.

To test the in vivo antitumor activity of each optimized sCAR-T, we first examined them in mouse xenograft models using Her2 3 + (HCC1954) and Her2 2 + (MDA-MB453) breast cancer tumors. Tumor cells (5×10^6) were inoculated subcutaneously in the right flank of NSG mice and solid tumors were grown until palpable (~ 300 mm³). The half-life

of Fabs in mice is approximately 1–2 h.[27] However, in MDA-MB435/Her2 tumor-bearing mice, we observed tumor distribution of IRDye800-Fab up to 72 h post intravenous (i.v.) injection, indicating excellent tumor residence of the relatively small Fab molecule (Figure S18). On day 10, mice were infused i.v. with 30×10^6 anti-FITC or anti-PNE sCAR-T cells, followed by i.v. injection of the corresponding switches every other day at 0.5 mg kg^{-1} for 14 days (total of 7 injections). Separately, control groups of sCAR-T cell-treated mice were dosed with wild-type 4D5 Fab. The conventional anti-Her2 CAR-T was included as a positive control. Tumor growth was monitored for 50 days. As shown in Figure 3 A and 3B, both conventional and sCAR-T cells exhibited comparable tumor regression kinetics and completely eliminated both Her2 3 + and 2 + tumors by day 25; no relapse was observed during the course of the study. Treatment of sCAR-T cells with wild-type 4D5 Fab had no effect on tumor growth. To test activity with lower antigen density Her2 1 + tumors, we used an orthotopic xenograft model with MDA-MB231 cells. In this model, 5×10^6 tumor cells were implanted into the right fourth mammary fat pad of female NSG mice to generate tumors. Ten days after tumor implantation, treatment was started with the same dosing and schedule as the Her2 3 + and 2 + models described above. As shown in Figure 3 C, sCAR-T cells fully eradicated Her2 1 + tumors by day 30, and no tumor relapse occurred during the 50 days of observation. The kinetics of tumor
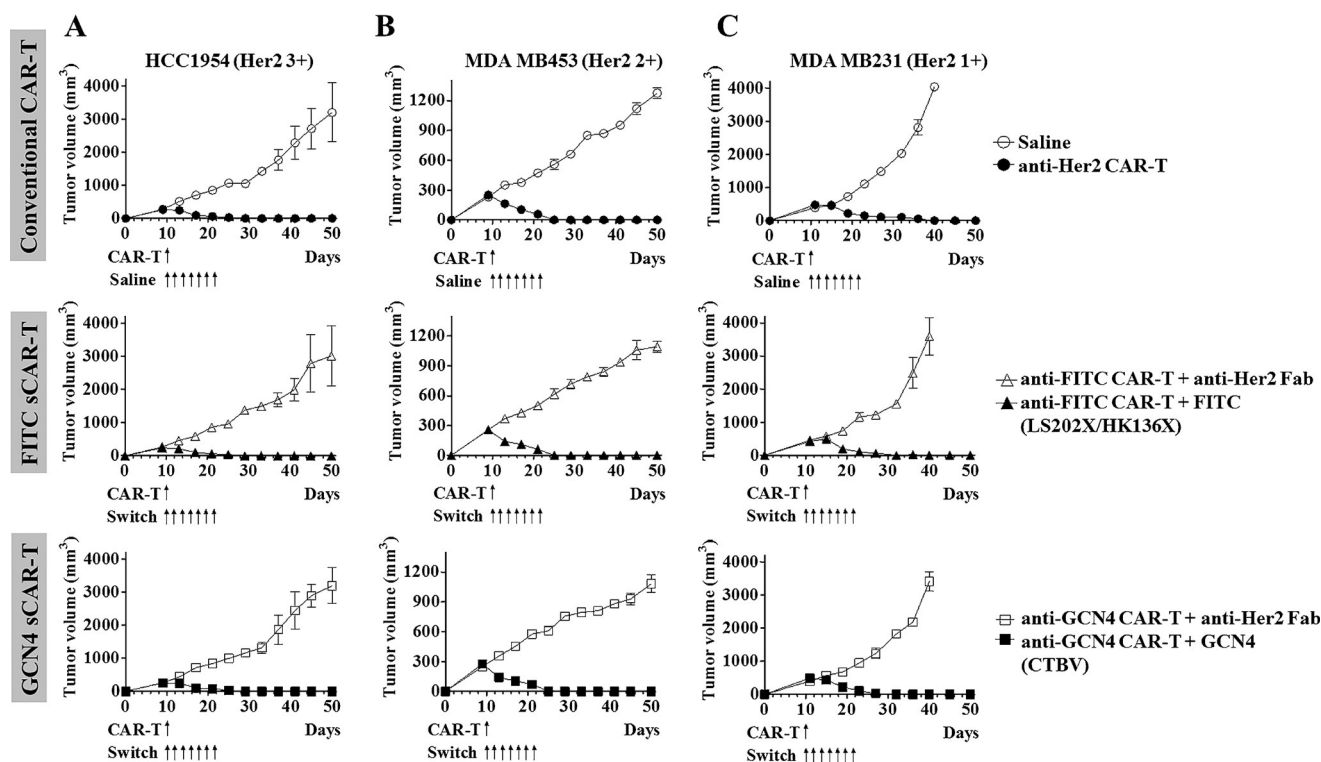
Figure 3. In vivo antitumor efficacy of conventional anti-Her2 CAR-T and sCAR-T cell approaches in HCC1954 (A), MDA-MB453 (B), and MDA-MB231 (C) xenograft models. For HCC1954 or MDA-MB453, 5×10^6 cancer cells were subcutaneously implanted in the right flank of female NSG mice. For MDA-MB231 cancer cells, 5×10^6 cells were orthotopically implanted into the right fourth mammary fat pad of female NSG mice. Ten days later, the mice were i.v. injected with 30×10^6 CAR-T cells, followed by the dosage of switch or wild-type 4D5 Fab at 0.5 mg kg^{-1} every other day for 14 days. The control group received saline instead of switch and did not receive any T cells. Tumors were measured twice a week with calipers and tumor volume was calculated by W×L×H. Each data point represents tumor volume of five mice in each group. Error bars represent SD. Arrows indicate the time of CAR-T cell injection or of treatment with specific switches.

clearance were comparable to that of conventional anti-Her2 CAR-T cells. These results show that sCAR-T cells constructed with different designs can specifically target and eliminate Her2-expressing tumors with comparable efficacy to a conventional CAR-T approach. Although additional studies are required to determine the optimal dosing regimen, tumor distribution, persistence, and other factors that affect CAR-T cell safety and efficacy, we believe these studies will facilitate the application of CAR-T therapy to solid tumors for which monoclonal antibody or antibody–drug conjugate therapies are not effective.

[1] D. M. Barrett, N. Singh, D. L. Porter, S. A. Grupp, C. H. June, *Annu. Rev. Med.* **2014**, *65*, 333–347.

[2] B. Jena, G. Dotti, L. J. Cooper, *Blood* **2010**, *116*, 1035–1044.

[3] N. P. Restifo, M. E. Dudley, S. A. Rosenberg, *Nat. Rev. Immunol.* **2012**, *12*, 269–281.

[4] S. A. Grupp, M. Kalos, D. Barrett, R. Aplenc, D. L. Porter, S. R. Rheingold, D. T. Teachey, A. Chew, B. Hauck, J. F. Wright, M. C. Milone, B. L. Levine, C. H. June, *N. Engl. J. Med.* **2013**, *368*, 1509–1518.

[5] C. U. Louis, B. Savoldo, G. Dotti, M. Pule, E. Yvon, G. D. Myers, C. Rossig, H. V. Russell, O. Diouf, E. Liu, H. Liu, M. F. Wu, A. P. Gee, Z. Mei, C. M. Rooney, H. E. Heslop, M. K. Brenner, *Blood* **2011**, *118*, 6050–6056.

[6] S. A. Rosenberg, J. C. Yang, R. M. Sherry, U. S. Kammula, M. S. Hughes, G. Q. Phan, D. E. Citrin, N. P. Restifo, P. F. Robbins, J. R. Wunderlich, K. E. Morton, C. M. Laurencot, S. M. Steinberg, D. E. White, M. E. Dudley, *Clin. Cancer Res.* **2011**, *17*, 4550–4557.

[7] B. G. Till, M. C. Jensen, J. Wang, X. Qian, A. K. Gopal, D. G. Maloney, C. G. Lindgren, Y. Lin, J. M. Pagel, L. E. Budde, A. Raubitschek, S. J. Forman, P. D. Greenberg, S. R. Riddell, O. W. Press, *Blood* **2012**, *119*, 3940–3950.

[8] S. L. Maude, N. Frey, P. A. Shaw, R. Aplenc, D. M. Barrett, N. J. Bunin, A. Chew, V. E. Gonzalez, Z. Zheng, S. F. Lacey, Y. D. Mahnke, J. J. Melenhorst, S. R. Rheingold, A. Shen, D. T. Teachey, B. L. Levine, C. H. June, D. L. Porter, S. A. Grupp, *N. Engl. J. Med.* **2014**, *371*, 1507–1517.

[9] D. L. Porter, W. T. Hwang, N. V. Frey, S. F. Lacey, P. A. Shaw, A. W. Loren, A. Bagg, K. T. Marcucci, A. Shen, V. Gonzalez, D. Ambrose, S. A. Grupp, A. Chew, Z. Zheng, M. C. Milone, B. L. Levine, J. J. Melenhorst, C. H. June, *Sci. Transl. Med.* **2015**, *7*, 303ra139.

[10] R. A. Morgan, J. C. Yang, M. Kitano, M. E. Dudley, C. M. Laurencot, S. A. Rosenberg, *Mol. Ther.* **2010**, *18*, 843–851.

[11] S. Kakarla, S. Gottschalk, *Cancer J.* **2014**, *20*, 151–155.

[12] M. Chmielewski, H. Abken, *Expert Opin. Biol. Ther.* **2015**, *15*, 1145–1154.

[13] T. Gargett, M. P. Brown, *Front Pharmacol.* **2014**, *5*, 235.

[14] M. S. Kim, J. S. Ma, H. Yun, Y. Cao, J. Y. Kim, V. Chi, D. Wang, A. Woods, L. Sherwood, D. Caballero, J. Gonzalez, P. G. Schultz, T. S. Young, C. H. Kim, *J. Am. Chem. Soc.* **2015**, *137*, 2832–2835.

[15] J. S. Ma, J. Y. Kim, S. A. Kazane, S. H. Choi, H. Y. Yun, M. S. Kim, D. T. Rodgers, H. M. Pugh, O. Singer, S. B. Sun, B. R. Fonslow, J. N. Kochenderfer, T. M. Wright, P. G. Schultz, T. S. Young, C. H. Kim, Y. Cao, *Proc. Natl. Acad. Sci. USA* **2016**, *113*, E450—E458.

[16] D. T. Rodgers, M. Mazagova, E. N. Hampton, Y. Cao, N. S. Ramadoss, I. R. Hardy, A. Schulman, J. Du, F. Wang, O. Singer, J. Ma, V. Nunez, J. Shen, A. K. Woods, T. M. Wright, P. G. Schultz, C. H. Kim, T. S. Young, *Proc. Natl. Acad. Sci. USA* **2016**, *113*, E459-E468.

[17] K. Kudo, C. Imai, P. Lorenzini, T. Kamiya, K. Kono, A. M. Davidoff, W. J. Chng, D. Campana, *Cancer Res.* **2014**, *74*, 93–103.

[18] K. Tamada, D. Geng, Y. Sakoda, N. Bansal, R. Srivastava, Z. Li, E. Davila, *Clin. Cancer Res.* **2012**, *18*, 6436–6445.

[19] K. Urbanska, E. Lanitis, M. Poussin, R. C. Lynn, B. P. Gavin, S. Kelderman, J. Yu, N. Scholler, D. J. Powell, Jr., *Cancer Res.* **2012**, *72*, 1844–1852.

[20] J. Dommerholt, S. Schmidt, R. Temming, L. J. Hendriks, F. P. Rutjes, J. C. van Hest, D. J. Lefeber, P. Friedl, F. L. van Delft, *Angew. Chem. Int. Ed.* **2010**, *49*, 9422–9425; *Angew. Chem.* **2010**, *122*, 9612–9615.

[21] J. E. Hudak, R. M. Barfield, G. W. de Hart, P. Grob, E. Nogales, C. R. Bertozzi, D. Rabuka, *Angew. Chem. Int. Ed.* **2012**, *51*, 4161–4165; *Angew. Chem.* **2012**, *124*, 4237–4241.

[22] Y. Cao, J. Y. Axup, J. S. Ma, R. E. Wang, S. Choi, V. Tardif, R. K. Lim, H. M. Pugh, B. R. Lawson, G. Welzel, S. A. Kazane, Y. Sun, F. Tian, S. Srinagesh, T. Javahishvili, P. G. Schultz, C. H. Kim, *Angew. Chem. Int. Ed.* **2015**, *54*, 7022–7027; *Angew. Chem.* **2015**, *127*, 7128–7133.

[23] T. J. Vaughan, A. J. Williams, K. Pritchard, J. K. Osbourn, A. R. Pope, J. C. Earnshaw, J. McCafferty, R. A. Hodits, J. Wilton, K. S. Johnson, *Nat. Biotechnol.* **1996**, *14*, 309–314.

[24] C. Zahnd, S. Spinelli, B. Luginbuhl, P. Amstutz, C. Cambillau, A. Pluckthun, *J. Biol. Chem.* **2004**, *279*, 18870–18877.

[25] M. C. Milone, J. D. Fish, C. Carpenito, R. G. Carroll, G. K. Binder, D. Teachey, M. Samanta, M. Lakhal, B. Gloss, G. Danet-Desnoyers, D. Campana, J. L. Riley, S. A. Grupp, C. H. June, *Mol. Ther.* **2009**, *17*, 1453–1464.

[26] M. Sun, H. Shi, C. Liu, J. Liu, X. Liu, Y. Sun, *Breast Cancer Res.* **2014**, *16*, R61.

[27] A. Nguyen, A. E. Reyes, M. Zhang, P. McDonald, W. L. Wong, L. A. Damico, M. S. Dennis, *Protein Eng. Des. Sel.* **2006**, *19*, 291–297.